Fuel 303 (2021) 121271

Contents lists available at ScienceDirect

Fuel

journal homepage: www.elsevier.com/locate/fuel

Full Length Article

Steam O_2-enriched air gasification of lignite and solid recovered fuel in fluidized bed

Katia Gallucci [a,*], Andrea Di Giuliano [a], Sergio Rapagnà [b]

[a] Department of Industrial and Information Engineering and Economics, University of L'Aquila, Monteluco di Roio, Piazzale Pontieri, 1 67100, L'Aquila, Italy
[b] Faculty of Bioscience and Agro-Food and Environmental Technology, University of Teramo, Campus "Aurelio Saliceti", via R. Balzarini 1, 64100 Teramo, Italy

ARTICLE INFO

Keywords:
Lignite
Solid recovered fuel
Steam–O_2-enriched air gasification tests
Pressure-fluctuation signal

ABSTRACT

Continuous steady-state gasification tests were performed, in which mixtures of lignite and solid recovered fuel (SRF) were fed to a bench-scale facility at atmospheric pressure, loaded with the bottom product of a high-temperature Winkler gasifier as the fluidized bed material. The O_2/fuel and steam/fuel ratios were varied from 0.3 to 0.4 and from 0.25 to 0.35, respectively, and the effects of the temperature were examined at different levels (700, 750, and 800 °C). The objective of the experimental campaign was to evaluate the effects of above mentioned operating conditions on the (i) quality of syngas expressed in terms of gas yield (Y_{gas}), cold gas efficiency (η_{CG}), and carbon conversion (X_C); (ii) effectiveness in tar reduction; and (iii) improvement of the H_2/CO molar ratio. Characterization analyses (grain-size distribution, scanning electron microscopy and energy-dispersive X-ray spectroscopy) were performed on the materials before and after the tests. Pressure-fluctuation signals were acquired during the tests to monitor the fluidization quality and diagnose the correlated incipient sintering or agglomeration of the bed particles. At 800 °C, the obtained results (Y_{gas} = 1.53; η_{CG} = 79%; X_C = 92%;tar content = 7.35 g/Nm^3; H_2/CO molar ratio = 0.96) demonstrated the convenient feasibility of gasification with the SRF–lignite mixture as a fuel (SRF/lignite = 0.5 wt/wt) and helped define the operating conditions for future pilot tests aiming for liquid fuel synthesis, although the best results were obtained at 800 °C with SFR/lignite = 0.2 wt/wt (Y_{gas} = 1.79; η_{CG} = 93%; X_C = 102%;tar content = 0.92 g/Nm^3; H_2/CO molar ratio = 0.84).

1. Introduction

Mitigating climate change has become a necessity for the sustainable development of the economy and social world, with the objective of enhancing environmental protection despite the increasing energy demand [1–3]. Accordingly, the European Green Deal aims to boost the efficient use of resources by transitioning to a clean circular economy, restoring biodiversity, and reducing pollution, thereby promoting a new growth strategy that turns climate and environmental challenges into opportunities [4]. This green transition is planned to be inclusive; through the Just Transition Mechanism: financial support and technical assistance will be provided to the most vulnerable coal- and carbon-intensive regions [4,5].

The European Green Deal has set the final goal of EU climate neutrality by 2050 [4]. These inspiring principles, which are being renewed and reinforced, have already been pursued by the Research Fund for Coal and Steel (RFCS), which supports research activities concerning the coal sector in regions involved in the green transition, aiming to optimize the utilization and conservation of resources, taking into account the decarbonization of the energy sector [4]. In the RFCS framework, the LIG2LIQ project "Cost Effective Conversion of Lignite and Waste to Liquid Fuels" has been co-funded, and the study reported in this paper summarizes the achievements from one of its experimental tasks [6].

The diversion of materials from landfills is a dual environmental problem of decarbonization; accordingly, researchers have focused on the energetic and chemical valorization of municipal solid waste (MSW) and biogenic residues [7–10], because of their considerable energy potential. Among all the available techniques, gasification is the most promising and suitable option with regard to feedstock flexibility, efficiency, versatility of operating conditions [11–13], process intensification, and scalability [14–16]. The main product of gasification is syngas—a H_2-rich gas used for power generation in integrated gasification combined cycle (IGCC) systems [17–19] or high-efficiency fuel

* Corresponding author.
E-mail address: katia.gallucci@univaq.it (K. Gallucci).

https://doi.org/10.1016/j.fuel.2021.121271
Received 22 January 2021; Received in revised form 10 June 2021; Accepted 12 June 2021
Available online 22 June 2021
0016-2361/© 2021 The Authors. Published by Elsevier Ltd. This is an open access article under the CC BY-NC-ND license (http://creativecommons.org/licenses/by-nc-nd/4.0/).

cells [20,21], as well as for the synthesis of alternative fuels via catalytic reactions (e.g., hydrocarbons from the Fischer–Tropsch (FT) process, methanol, mixed alcohols, or substitute natural gas) [22–25].

Co-gasification technologies have generated increasing interest as a means of disposal with energy recovery. Yu et al. [26] experimentally investigated the co-gasification of biosolids (stabilized solids from wastewater treatment) with vegetal biomass, focusing on the catalytic effects on gasification due to potassium in the vegetal fuel and negative influences due to the increase in biosolid-fed fractions higher than 25%. Positive influences due to potassium from excess vegetal biomasses in co-gasification with fossil fuels were also examined via kinetic experiments in a thermogravimetric analyzer [27,28] and in a pilot-scale bubbling fluidized bed [29,30] at 800–860 °C or below 700 °C with *in situ* CO_2-capture in the presence of lime [31], with the excess biomass needed to compensate for the formation of inactive potassium aluminosilicates due to aluminosilicate minerals in coal [28].

Other studies [32–41] have focused on the feasibility of waste co-gasification with low-quality coal (lignite) and/or biomass. Nonetheless, to achieve good syngas quality, an adequate H_2/CO ratio, and efficient removal of tar and trace elements, as well as the possible integration of advanced hot gas cleaning systems, which would require technical feasibility in long-term runs under industrial operation [42], a dedicated experimental campaign must be conducted to investigate the peculiarities of different solid recovered fuels (SRFs,—i.e., homogeneous fuels obtained by processing MSW) [10,39,41,43,44]. An interesting option for the co-gasification process integrated with waste-to-energy production technologies was investigated at bench [37] and pilot [45] scales, with different feedstocks [46] or blending SRF with bio-residues [39], and fluidized bed gasifiers have emerged as the most suitable technology to prevent technical issues related to a feedstock with a high content of ash that exhibits a low melting point [47–51].

In a preliminary study by this research group [52], steam N_2-gasification tests were performed with both lignite and a blend of lignite and SRF (SRF/lignite = 0.25 wt/wt), in the same bench-scale fluidized-bed reactor employed in this study, using the same material to constitute the fluidized bed (i.e., bottom residual product of a high-temperature Winkler (HTW) gasifier [53]). Thus, the gasification conditions of a full-scale HTW plant were mimicked at a bench scale. The objective of this study was to investigate the behavior of two SRF/lignite mixtures for (i) determining the feasibility of tests in larger-scale apparatuses, (ii) identify the best realistic operating conditions for producing high-quality syngas (low tar content and high H_2 and CO fractions), and (iii) preventing undesirable plant shutdown. Important and novel contributions were introduced to the experimental methods, i.e., the addition of O_2 from the bottom of the reactor and the variation in the SRF/lignite weight ratio up to 0.5, under different operating conditions. All these investigations were dictated by the pursuit of the main goals of Work Package 2 of the LIG2LIQ project: *"to determine the design and operating conditions of the fluidized bed gasifier, optimized with regard to the cold gas efficiency (target: 82%), carbon conversion efficiency (target: 95%–98%), O_2 consumption, and operability, to test the suitability of the selected feedstock for fluidized bed gasification"* [6]. These laboratory-scale experiments were planned for the preliminary establishment of feasible operating conditions in a 0.5-MWth HTW gasification plant, which is the core of an economically efficient method for the production of valuable substances, such as FT fuels or methanol, from lignite, plastics, and biowastes. The laboratory-scale investigations of this study—particularly regarding the feedstock properties relevant for fluidized bed gasification—were necessary for setting the real conditions to be operated in the 0.5-MWth pilot plant, experimenting with specific ratios of co-gasified feedstocks, and identifying viable solutions for the main possible technical limitations. The entire experimentation to establish the feasibility of the LIG2LIQ process will subsequently require conducting long-term tests at the pilot scale.

2. Materials and methods

2.1. Experimental apparatus

A bench-scale (Fig. 1), externally heated, cylindrical stainless-steel fluidized-bed reactor (inner diameter = 100 mm, height = 850 mm) was used to perform the gasification experiments. The entire apparatus, which includes this reactor, has been described in detail elsewhere [52,54]. An additional gas line was employed in the present study to feed the O_2-enriched air, which was needed to investigate the entire range of operating conditions for LIG2LIQ Work Package 2 (see Table 2). Steam, nitrogen, and enriched air (50 vol% O_2 in N_2)—fed in different proportions—were used as gasification agents. The solid fuel was continuously fed into the reactor via a suitable screw feeder and a feeding probe (inner diameter = 13 mm) and purged with a small N_2 flow, helping the fall-down of the feedstock. A ceramic filter candle was placed in the freeboard above the fluidized bed: before leaving the gasifier, the raw product gas was forced to pass through the candle pores, allowing the production of practically dust-free syngas [55]. After the cooling/condensation section, the flow rate of the dry product gas was measured, and its composition was determined using online gas analyzers. A slipstream of the produced gas was sent to the tar sampling unit, according to the specifications of the CEN/TS 15439:2006 standard [56], and the liquid tar samples collected in the impinger bottles were analyzed offline via high-pressure liquid chromatography (HPLC, Hitachi "Elite LaChrom" L-2130) for the detection and quantification of heavy hydrocarbons in the product gas. Detectable tar compounds representative of the typical tar composition, as well as the related analytical method, were reported in [57]. A second slipstream of the gas was sent to online gas analyzers (ABB IR-URAS 14, TCD-CALDOS 17, and IR-SIEMENS ULTRAMAT 6), which measured the concentrations of H_2, CO, CO_2, CH_4, and NH_3. The temperatures in the reactor bed, freeboard, and outlet of the filter candle (reactor top) were measured and recorded.

A vertical probe in the freeboard was connected to a piezoelectric KISTLER transducer for pressure-fluctuation signal acquisition. The transformed voltage signal was amplified, digitally converted, and stored in a personal computer, on which a tailored LABVIEW® routine was installed. The choice of the proper sampling frequency and duration of each acquisition is discussed elsewhere [5859]. For each stored signal, the analysis of the power spectral density function (PSDF) and standard deviation (related to the number of erupting bubbles and their size at the bed surface [59]) was used as a diagnostic method to evaluate the fluidization quality and promptly detect incipient sintering in the bed. This online measuring method may represent an alternative to the Early Agglomeration Recognition System, which compares pressure time-series (high-frequency pressure measurements from the fluidized bed) in a statistical manner, using nonlinear analysis techniques based on principal component analysis, and is widely capable to visually distinguish the agglomeration condition from a well-fluidized reference condition [60–62].

The morphological properties and local elemental composition of the feedstock fuels and bed material—before and after the tests—were investigated using scanning electron microscopy and energy-dispersive X-ray spectroscopy (SEM-EDS). The analyses were performed using a field-emission analyzer (ZEISS Gemini 500 SEM, acceleration voltage ranging from 0.02 to 30 kV; store resolution up to 32 k × 24 k pixels—0.6 nm at 15 kV, in backscattering electron mode; pressure ranging from 5 to 500 Pa) equipped with an EDS microanalyzer (OXFORD Aztec Energy) and an INCA X-ACT PELTIER COOLED ADD detector. All the samples were coated with 5 nm of Cr in an automatic sputter coater (Q 150 T ES).

The grain-size distribution of the samples was determined using an optical instrument (Mastersizer 2000, Malvern). Each sample underwent grain-size analysis after the manual coning quartering procedure. The grain-size distribution was also determined for some of the samples

A bench-scale (

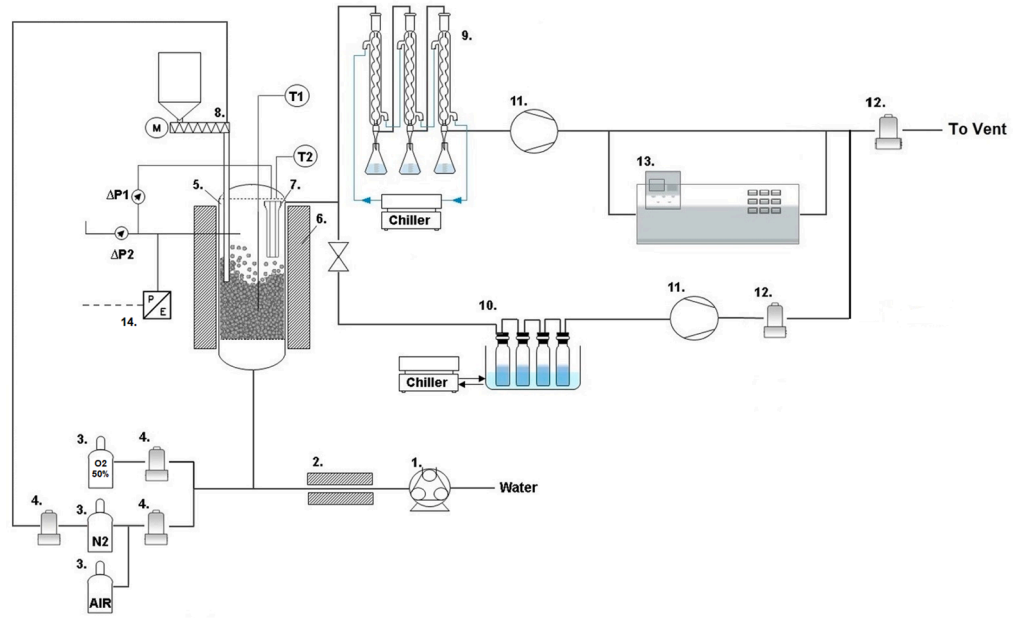

Fig. 1. Sketch of the bench-scale fluidized bed apparatus (modified and). adapted from [52]

before and after the tests.

2.2. Materials

Pre-dried Rhenish lignite (LEG) was the main feedstock, kindly supplied by RWE AG; its ultimate analysis was detailed in [52] and is recalled here for convenience (Table 1). In this study, LEG was fed alone or blended with SRF supplied by N + P (Subcoal®).

The chemical compositions of the ashes are presented in Tables S1 and S2 (Supporting Information).

The fluidized bed was made of HTW bottom product, that is, the solid residue of LEG gasification performed in an HTW pilot-scale plant [63], mainly composed of char (74.35 wt% C on a dry basis) and ashes (almost three times the content of original LEG) [63].

The particle-size distributions of the LEG and HTW bottom products before use were reported in [52]; the Sauter particle diameters $d_{3,2}$ were 20.66 and 441.93 μm, respectively.

Table 1
Characterization analyses of LEG, SRF provided by Institute for Chemical Processing of Coal (ICHPW), Poland (values ± uncertainty estimated for k = 2 and confidence level 0.95).

	LEG	SRF
Total moisture content (wt%)	10.6 ± 0.3	3.3 ± 0.3
Ash content (dry basis) (wt%)	3.8 ± 0.2	14.4 ± 0.8
Volatile matter (dry basis) (wt%)	50.31 ± 0.19	76.3 ± 0.7
C (dry basis) (wt%)	67.3 ± 0.5	53.7 ± 0.5
H (dry basis) (wt%)	4.79 ± 0.10	7.65 ± 0.08
N (dry basis) (wt%)	0.84 ± 0.03	0.59 ± 0.08
S (dry basis) (wt%)	0.35 ± 0.05	0.21 ± 0.04
Cl (dry basis) (wt%)	0.02 ± 0.01	1.9 ± 0.4
Ash fusion temperature:Deformation temperature (°C)	960 ± 16	1240 ± 13
Ash fusion temperature:Flow temperature (°C)	1490 ± 19	1280 ± 12

2.3. Operating conditions

The adopted set points of the operating conditions are presented in Table 2, which were selected to investigate at bench scale the feeding of SRF/LEG mixtures into an HTW gasifier, for verifying its feasibility and optimizing related parameters.

The combination of tests #1 and #6–#11 (Table 2) allowed the estimation of the effects of each relevant parameter on the produced syngas, independently; tests #2–#5 (grey cells in Table 2) constituted a first attempt of four consecutive tests with an SRF/LEG ratio of 0.2 wt/wt using roughly ground SFR material. A new grinding method was applied to the SRF pellets in tests #6–#11: they were finely ground with a RETSCH Mühle Stainless Steel Bottom Sieve (pore size of 1.00 mm) to obtain a wooly material. The experimental conditions of failed tests #2–#5 were successfully repeated with this new SRF for tests #6–#9 (Table 2). The failed tests are discussed in Supporting Information (S2. Main issues and applied solutions) to highlight interesting aspects of the experiments.

For the tests at the highest SRF/LEG ratio (tests #10 and #11 in Table 2), the original screw feeder of the test rig had to be replaced by a screw with deeper blades and a larger pitch to better push the soft SRF/LEG mixture.

2.4. Analysis of products

The water conversion η_{wc}(%) was calculated as

$$\eta_{wc} = \frac{\dot{m}_{water,in} + \dot{m}_{fuel\_moisture,in} - \dot{m}_{water,out}}{\dot{m}_{water,in} + \dot{m}_{fuel\_moisture,in}} \times 100, \quad (1)$$

where $\dot{m}_{water,in}$ and $\dot{m}_{water,out}$ represent the mass flow rates of water input and output (collected in condenser flasks), respectively, and $\dot{m}_{fuel\_moisture,in}$ represents the water feeding due to the moisture in the

Table 2
Operating conditions of the test campaign for steam O_2-enriched air gasification.

Test	#1	#2	#3	#4	#5	#6	#7	#8	#9	#10	#11
Bed material	HTW bottom product										
Feedstock	LEG	LEG + SRF									
SRF/LEG (wt/wt)	0	0.2				0.2				0.5	
Feed rate (g/min)	10.7	10.4*				9.82				10.4	
Nominal temperature (°C)	750	700	750	750	800	700	750	750	800	750	800
Steam/fuel (g/g)	0.25	0.25	0.25	0.30	0.35	0.25	0.25	0.30	0.35	0.25	0.35
O_2/fuel (g/g)	0.3	0.3	0.3	0.35	0.4	0.3	0.3	0.35	0.4	0.3	0.4

*nominal but did not occur, see Supporting Information (S2. Main issues and applied solutions)

solid feedstock fuel.

The quantity of dry product gas, which was measured using a mass flow meter, allowed the calculation of the gas yield $Y_{gas}\left(\mathrm{Nm^3/kg_{fuel}}\right)$:

$$Y_{gas} = \frac{F_{gas,out}}{F_{fuel,in}}, \tag{2}$$

where $F_{gas,out}$ represents the total dry N_2-free volume (at normal conditions) gas flow produced, and $F_{fuel,in}$ represents the mass flow of the input feedstock fuel.

The cold gas efficiency $\eta_{CG}(\%)$ is calculated as

$$\eta_{CG} = \frac{LHV_{gas}F_{gas,out}}{LHV_{fuel}F_{fuel,in}} \times 100, \tag{3}$$

where LHV_{gas} and LHV_{fuel} are the lower heating values of the produced gas and fuel expressed in MJ/Nm^3 and MJ/kg, respectively.

The carbon conversion $X_C(\%)$ is defined as

$$X_C = \frac{\sum n_i}{n_{C_{in}}} \times 100, \tag{4}$$

where n_i represents the number of moles of the i carbonaceous species in the product gas (CO, CO_2, CH_4), from the analysis of the gas composition, and $n_{C_{in}}$ represents the number of moles of C in the feedstock input.

With the HTW bottom product as the bed material, the global mass balance could be verified every time the bed was unloaded and weighed (subtracting the accumulated ashes in the bed) after a certain number of tests were performed with the same feedstock; alternatively, it could be estimated by assuming that the missing carbon in the mass balance of each single test was ascribable to the char (the only non-measured variable).

3. Results and discussion

3.1. Analysis of materials pre-test

One of the differences introduced in this test campaign relative to the aforementioned preliminary work on SRF [52] was the grinding of the SRF pellets using a professional RETSCH mill equipped with a stainless-steel bottom sieve having a pore size of 1.00 mm. This operation resulted in a narrow distribution of SRF particle dimensions, centered around 1 mm (e.g., for the SRF/LEG = 0.5 in Fig. 5), whereas the LEG fine powder, whose sizes ranged from 1 to 200 μm, exhibited a smaller Sauter particle diameter ($d_{3,2}$) of 45.3 μm.

Interesting morphological details of the SRF-LEG mixture emerged from SEM-EDS analysis, and the filamentous aspect of the SRF appeared as the main feature of the sample, although LEG particles, which resembled stones, were visible as well (Fig. 2a). At a higher magnification, the SRF appeared to be reduced to thin strips 10–30 μm in width, with the fine fraction of LEG covering these wires similarly to dust (Fig. 2). With the naked eye, the mixture appeared completely black as LEG (while solo-SRF after grinding has a heterogeneous pigmentation within a gray matrix and macroscopically appears as a low-density fluff).

The local EDS analyses of specific zones of this sample (Fig. 3) indicated that C and O were the most diffuse elements but also highlighted the chemical heterogeneity of the sample. The EDS spectra were not superimposable, and numerous elements (Na, Mg, Fe, S, Cl, Si Al, K, Ti) were only locally detected. In addition to C and O, Na, and Mg were present in all the spectra, except for spectrum 120 (Fig. 3); spectrum 121 (Fig. 3) suggested the presence of an aluminosilicate, in accordance with a previous ICP-OES analysis [52], which revealed Ca, S, Mg, and Fe to be the main elements in the LEG ashes, whereas Si, Ca, and Al were identified in SRF ashes, with a low content of SO_3 (<3 wt%). Despite the small amounts of K and Na, these low-melting point elements can promote bed agglomeration in the presence of silica [64]. The omnipresent unidentified consecutive peaks in Fig. 3 corresponded to Cr, which was present because of vapors added to metallize the nonconductive surfaces (sputtering procedure for SEM-EDS).

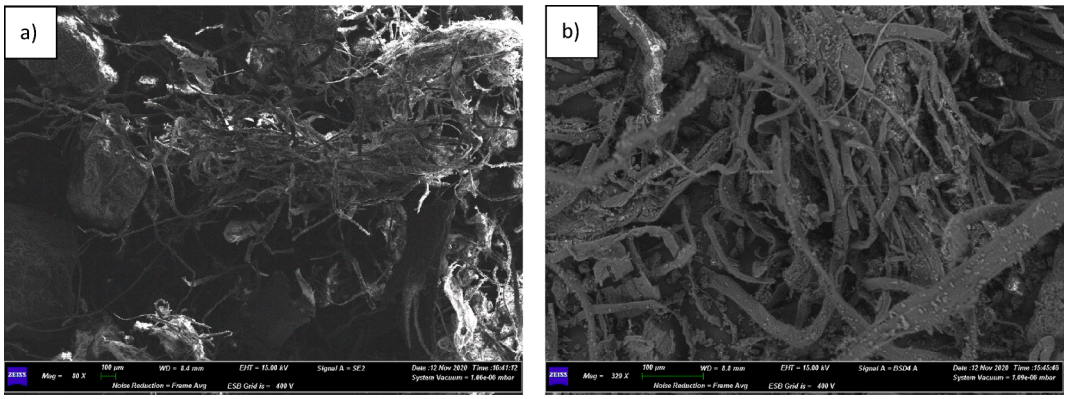

Fig. 2. SEM images of SRF/LEG = 0.5 at different magnifications: (a) overview of sample at 80×; (b) details of the filamentous tangle and fine carbonaceous particles on the SRF (329 ×).

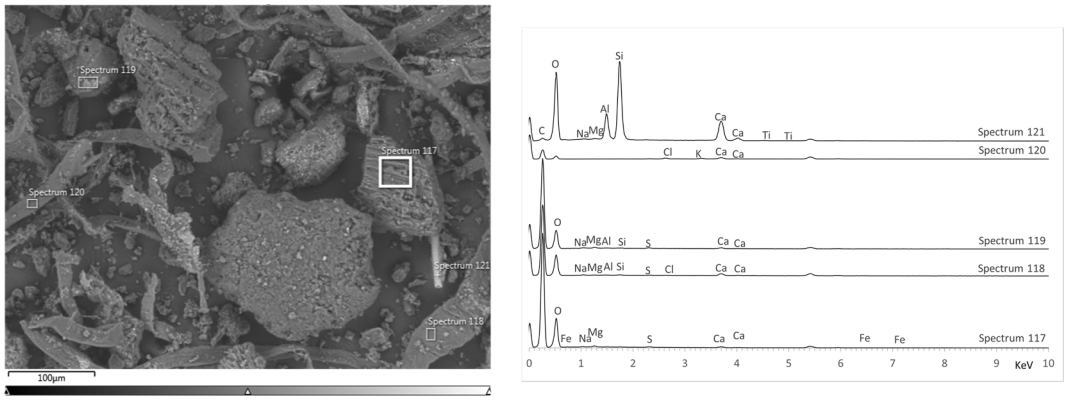

Fig. 3. Local EDS analyses of SRF/LEG = 0.5 samples.

3.2. Gasification results

The main parameters investigated were the inlet content of O_2, steam/fuel ratio, temperature, and SRF/LEG ratio, as shown in Table 2.

Test #1 was performed with LEG alone (SRF/LEG = 0), as the reference test for the entire set of experiments. As mentioned in Subsection 2.3, the first attempt of four consecutive tests (#2, #3, #4, #5) with an SRF/LEG ratio of 0.2 caused clogging of the fuel vertical feeding probe. Insight into the operational issues encountered and solutions adopted is provided in the Supporting Information (S2. Main issues and applied solutions. The blockage of SRF/lignite feeding that occurred in the elbow fitting between the horizontal screw feeder and the vertical probe, together with the continuous external heat supply to the bed of HTW bottom products, produced pyrolysis until the exhaustion of the volatile material and finally caused the overheating and consequent sintering of the ashes in the bed (Fig. S1).

The main results of the successful tests (#1 and #6–#11) are presented in Table 3.

The syngas composition of test #1 (Fig. 4a) was stable, with a slight increase in the content of hydrogen when the freeboard temperature was slightly reduced, probably because of the increased extent (albeit contained) of the endothermic water gas and reforming reactions and the resulting slight progression of the water gas shift reaction toward products. The immediate change in the gas composition, together with the estimated gas residence time in the reactor of approximately 5 s (on the same order of magnitude as those of previous works [52,65]), under the same experimental setup and similar operating conditions confirms that the test duration in the range of 30–60 min is appropriate to guarantee the gasification of the solid feedstock in the bed and the reforming reactions in the gas phase in the freeboard [66]. Under these operating conditions, a practically unitary H_2/CO ratio was achieved. The degree of water conversion η_{wc} was higher than that in homologous tests of the previous campaign [54], despite the combustion of the H_2 in the syngas due to fed O_2; this is easily explained by the fact that the steam/fuel ratio in the present case was 0.25, whereas it reached 0.65 in the tests of [54]. Conversely, the absence of O_2 in the feeding gas of the first test of [52] resulted in higher degree of water conversion and a larger H_2 yield.

The presence of SRF in the feed increased the H_2/CO ratio to 1.32 at a nominal temperature of 700 °C (test #6 in Table 3), which favored the formation of CO_2 via exothermic oxidation processes. In general, the relationship between the presence of SRF and the increase in the CH_4 content in the produced syngas (Table 3) was confirmed, which was ascribed to plastic material introduced to the fuel mixture by the SRF. After the first 15 min of test #6 and after some preliminary attempts (which introduced a larger amount of steam than the original set point), the first feeding problems were observed because of the sudden fluctuations of the main monitored variables, such as the syngas flow rate and

Table 3
Test results for steam O_2-enriched air gasification.

Test	#1	#6	#7	#8	#9	#10	#11
Feedstock	LEG	SRF/LEG = 0.2 wt/wt				SRF/LEG = 0.5 wt/wt	
Measured/actual process parameter (±95% confidence interval for averaged values)							
Bed temperature (°C)	762.3 ± 1.1	719.7 ± 0.6	759.2 ± 0.1	753.4 ± 0.1	816.5 ± 0.4	751.5 ± 0.6	797.0 ± 0.2
Freeboard temperature (°C)	752.2 ± 3.8	688.0 ± 0.7	735.1 ± 0.3	718.0 ± 0.03	783.8 ± 1.3	689.9 ± 1.1	756.2 ± 1.7
Steam/fuel (g/g)	0.25	0.25	0.26	0.32	0.34	0.25	0.33
O_2-N_2 (50%$_{vol}$) (Nl/min)	4.52	4.13	4.13	4.81	5.50	4.28	5.71
Test duration (min)	117	50	26	35	36	41	37
Main cumulative indices of quality syngas							
η_{wc}(%)	71.5	39.8	56.8	60.4	85.6	50.0	57.7
C conversion (%)	67.7	62.2	67.0	79.1	102	77.4	92.0
Char residue (g/kg)*	321	252	249	177	66.8	94.2	87.3
Gas yield (Nm^3/kg)	1.22	1.14	1.22	1.39	1.79	1.31	1.53
η_{CG}(%)	59.4	52.8	60.0	67.7	92.9	64.9	79.1
H_2 (Nl/min)	5.07	4.51	4.72	7.25	9.07	5.83	7.35
H_2 ($Nl/g_{feed\ daf}$)	0.52	0.46	0.48	0.52	0.66	0.49	0.55
Tar content HPLC (g/Nm^3)	6.74	2.39	n.d*	1.79	0.92	8.13	7.40
*estimated Average gas composition (vol% on dry and N_2 free basis) ± 95% confidence interval							
H_2 (vol%) dryN_2free	38.74 ± 0.03	40.46 ± 0.05	39.59 ± 0.11	38.31 ± 0.06	37.60 ± 0.06	37.93 ± 0.12	36.56 ± 0.13
CO (vol%) dryN_2free	38.37 ± 0.03	30.12 ± 0.06	35.50 ± 0.18	34.74 ± 0.07	44.70 ± 0.09	30.08 ± 0.15	37.91 ± 0.19
CO_2 (vol%) dryN_2free	17.90 ± 0.06	22.84 ± 0.05	18.29 ± 0.14	20.31 ± 0.02	12.01 ± 0.06	22.88 ± 0.07	17.42 ± 0.08
CH_4 (vol%) dryN_2free	5.64 ± 0.02	6.57 ± 0.02	6.62 ± 0.05	6.64 ± 0.02	5.62 ± 0.02	9.12 ± 0.10	8.11 ± 0.10
NH_3 (ppm) dryN_2free	1278 ± 5	1757 ± 15	1587 ± 28	2245 ± 33	1241 ± 21	2946 ± 92	2715.5 ± 75

*n.d. = not determined.

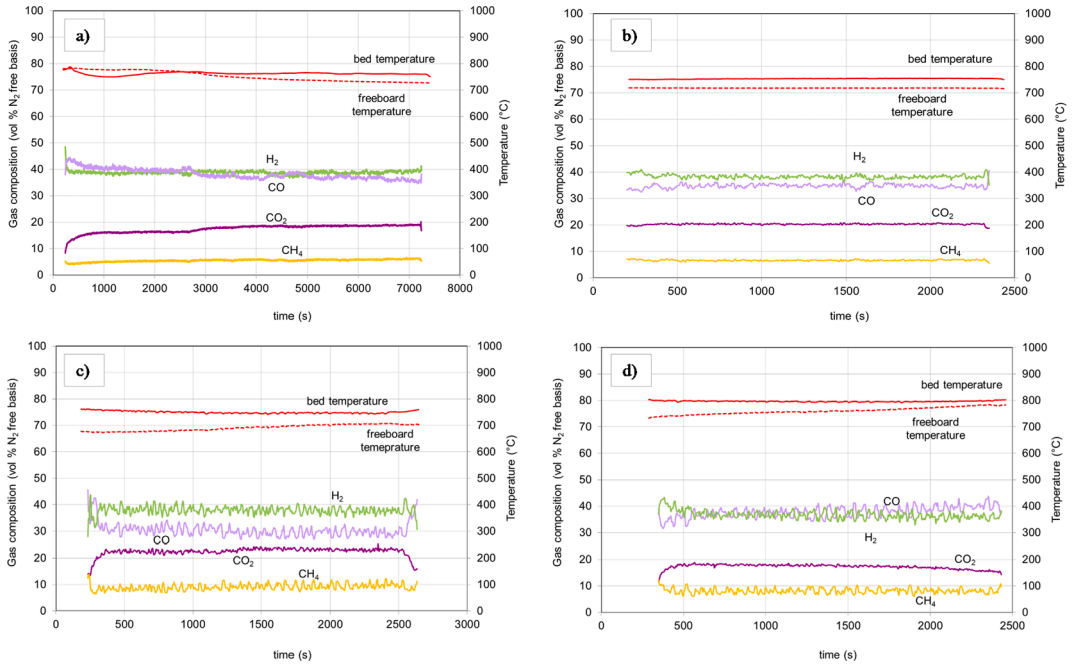

Fig. 4. Gas composition of main gas component on dry-N_2 free basis with temperature profiles in the bed and in the freeboard: (a) test #1; (b) test #8; (c) test #10; (d) test #11.

composition. This behavior was probably related to the softening of the SRF and the downy appearance and electrostatic nature of the prepared fuel mixture. The issue was promptly remedied by hammering the feeding probe repeatedly in tests #6-#9. This issue imposed the need for tests of reduced duration (tests #6–#11), ensuring in any case that outlet flow rates and compositions reached their stabilities and that correct tar sampling was allowed, according to the specifications of the CEN/TS 15439:2006 standard (at least 30 min, except for test #7, as discussed in the Supporting Information).

Test #8 exhibited a stable syngas composition, with a remarkably high H_2 content (Fig. 4b). However, with regard to the gas yield and H_2 flow rate, test #9 (conducted at a nominal temperature of 800 °C, Table 2) exhibited even better results (Table 3). Test #9 exhibited the highest efficiency among the whole series of tests, even though it was accompanied by an excessive carbon conversion value (102%). Initially, this odd value was ascribed to the higher temperature level of test #9, which may have increased the reactivity of the C present in the bed (HTW bottom product) and the C fed with the fuel mixture. Nevertheless, when the residue in the fuel dispenser was weighed *a posteriori*, a more plausible explanation emerged. It appeared that more LEGSRF mixture was fed than the supposed amount for tests #6–#9, according to the hypothesized nominal feeding rate of solid fuel; the fed excess amount of fuel (cumulatively for tests #6–#9, including intermediate warm-ups) was estimated to be 7.7% larger than the nominal value. With this in mind, we recalculated the carbon conversion and cold gas efficiency and obtained values on the order of 95% and 86%, respectively. Thus, if more LEG-SRF mixture was indeed fed, test #9 would remain the best test of the entire set. In contrast, the difference between the bed mass unloaded after test #9 and that loaded at the beginning of this four-test series (tests #6–#9) is only 102 g, of which 88.1 g is attributable to the accumulation of ashes. This indicates that the bed was not actually consumed, or that there was a renewal of bed material due to residues of the continuously supplied fuel, in contrast to the previous four unsuccessful attempts (tests #2–#5). The appearance of the discharged material after test #9 did not suggest the occurrence of lump formation or other significant sintering phenomena.

These doubts regarding the regularity of feeding further justify the replacement of the screw feeder for tests #10 and #11, in which the feeding difficulties related to the higher SRF content of 33.3% (corresponding to SRF/LEG = 0.5) could have been even more prominent. After a new calibration of the feeding system, tests #10 and #11 were performed for comparison with the homologous tests with an SRF/LEG ratio of 0.2 wt/wt (tests #8 and #9). In the last two tests, the higher operating temperature yielded promising results, with carbon conversions on the order of 92% and a cold gas efficiency of > 79% (see Table 3).

A comparison between tests #10 (Fig. 4c) and #11 (Fig. 4d) revealed better performance under the conditions of test #11 (see Table 3), with regard to the gas yield, cold gas efficiency, and carbon conversion. This was ascribed to the higher temperature, higher steam/fuel ratio (0.25 vs. 0.33,), and the O_2/fuel ratio, which was set as 0.4 (see Table 2). The O_2/fuel ratio of 0.4 significantly reduced the H_2/CO ratio from 1.2 to 0.95 via a reverse water gas shift, although a more extensive production of H_2 was observed in absolute terms for test #11 (Table 3): 5.83 vs. 7.35 Nl/min. This effect is ascribed to the steam/fuel ratio and the consequent enhancement of the gas–water reaction and reforming reactions due to the higher temperature set point, which also induced a greater H_2 release due to plastic fraction decomposition. As mentioned previously, a non-negligible increase in the CH_4 content was observed for the two last tests, relative to homologous tests conducted at the same temperature (i.e., test # 10 vs. tests # 1 and # 8, test # 11 vs. test # 9). Because of the increase in CH_4 (and tar content) correlated to the higher SRF fraction in the fuel feed, it is fair to expect an increase in the contents of light hydrocarbon species such as ethylene, ethane, or acetylene (although these were not directly measured), as previously reported [67–69]. However, it can be assumed that these compounds are not in significant quantities, thanks to the appreciable content of hydrogen measured in the produced gas. Despite the stronger fluctuations due to both the larger screw feeder and the different nature of the fuel (a higher SRF content and therefore a higher volatile content), the control of the feeding and the verification of the accumulation of ashes led to corroborating conclusions in the last two tests: an additional 80.5 g was found in the bed after test #11, compared with an estimated ash accumulation of 56.8 g in both tests #10 and #11. Regarding the feeding, the difference between the initial and final masses of the fuel material in the dispenser was measured, which was close to the value expected

according to the nominal feeding rate (different by only a few grams, corresponding to an error of < 1% when estimating the fuel flow rate). Ultimately, all the adopted strategies have proven effective and demonstrated the feasibility of HTW gasification with mixed SRF–lignite as the fed solid fuel, up to 33.3% by weight of the SRF, ensuring acceptable quality of the syngas without insurmountable management problems.

The production of NH_3 (ppm on an N_2-free basis in Table 3) was minimal for test #1 with LEG alone, even though the temperature was relatively low, whereas it exhibited a decreasing trend as the temperature was increased in tests #6–#9, probably owing to decomposition/oxidation effects. In contrast, an increase in the percentage of SRF unequivocally produced an increase in the content of NH_3, even though the maximum value remained well below 0.3 vol% (compare NH_3 results from test #1 with those from #6–#9 and #10 and #11 series in Table 3).

In the tests with SRF/LEG = 0.5, the tar content and CH_4 and CO_2 concentrations were slightly higher, probably because of the increased plastic fraction in the feed. For this reason, under similar conditions, the H_2 production was slightly improved as well (at 750 °C, 5.83 Nl/min in test #10 with SRF/LEG = 0.5 vs. 5.07 Nl/min in test #1 with LEG alone), and the NH_3 content increased from approximately 0.13 to approximately 0.29 vol% (the maximum measured value). Although it was impossible to directly measure the concentration of sulfur compounds, according to the elemental composition of LEG and SRF and experimental experience from previous studies [52], it is reasonable to assume that it did not exceed 0.05–0.1 vol% on a dry and nitrogen-free basis.

The tar content obtained in test #1 was higher than those obtained at the same temperature in previously reported tests [54] (2.5 g/Nm^3 of syngas with an olivine bed and triple the amount of steam) and from the first test in [52] (approximately 2 g/Nm^3 of syngas with a bed of HTW bottom product and steam/fuel = 0.6). By reasonably assuming that there was no contamination due to entrained fine carbonaceous particles, able to pass through the whole barrier of the filter candle, we can ascribe the lower tar contents obtained in the aforementioned tests [52,54] to the larger amounts of excess water, which promoted the reforming reactions under similar operating conditions. The measured slipstream during the tar sampling was unexpectedly small, which resulted in an overestimation of the tar concentration in the produced gas.

In contrast, the tar measurements for all the tests with SRF/LEG = 0.2 were satisfyingly low and improved as the temperature was increased, down to a minimum of 0.92 g/Nm^3 of syngas (the tar analysis of test #7 in Table 3 cannot be considered valid), which confirms that the presence of oxygen under these conditions is effective for reducing the tar content. This excellent result is ascribed to the synergistic effect of SRF/LEG co-gasification. Their ultimate, proximate, and ash analyses (see Tables 1 and Table S1 in Supporting Information) indicated the higher volatile-matter and H_2 contents of SRF, which increased the hydrogen content, cold gas efficiency, carbon conversion, and gas yield and enhanced the catalytic effect of LEG ashes containing alkaline earth metals and iron, promoting tar reforming [70] and sulfur capture [52,54]. However, a limited Na-K content in the SFR ashes, which contributes to the catalytic effect, ensures a high melting temperature of these materials and prevents sintering of these suitable and compatible materials for co-gasification processes.

The tar concentrations returned to high values when the SRF/LEG ratio was set as 0.5; under this condition, the 50 °C increase (from test #10 to test #11) reduced the tar content from 8.13 to 7.40 g/Nm^3. In all the tests with SRF/LEG = 0.2 (tests #6–#9 in Table 3), toluene and low-molecular-weight aromatics were the main components of the tar; in contrast, when the SRF content was increased (tests #10 and #11), the main components became acenaphthylene and acenaphthene, and it is plausible that some components of SRF (or SRF ashes) can favor the polymerization of the light aromatic compounds. The details of the HPLC analysis are presented in the Supporting Information (S3. HPLC analysis of tar sampling in 2-propanol.

3.3. Post-test analysis of materials

Granulometric analyses were performed on the recovered bed material after tests #10 and #11 (green solid curve, Fig. 5), as well as on char and fly ashes recovered on the filter candle surface (orange solid curve, Fig. 5). A comparison of these results with those for fresh fuel and bed materials (dotted lines, Fig. 5) indicated the almost complete gasification of SRF, which can be inferred from the disappearance of the maximum in the blue dotted curve of the original SRF-LEG distribution. Additionally, by comparing the original HTW bottom product (brown dotted curve, Fig. 5) to its post-test version (green solid curve, Fig. 5), a relevant formation of finer particles due to gasification can be inferred: the average $d_{3,2}$ diameter of the post-test HTW bottom product was significantly reduced to 60.6 μm, but the maximum of its distribution was still clustered around 400–500 μm, and the reduced $d_{3,2}$ value is ascribed to the spread shoulder on the left side of the distribution (green solid curve, Fig. 5).

The almost complete consumption of SRF in tests #10 and #11, which was probably due to the high contents of volatile matter, is confirmed by the SEM images in Fig. 6a and 6b, where the SRF residues are rare and extremely reduced in size, appearing among particles of HTW bottom product or gasified LEG. These stone-like particles of the bed exhibited a porous surface after the gaseous phase release (see Fig. 6 c) and, undoubtedly on the basis of SEM micrographs, they seemed no affected by agglomeration or sintering phenomena: this evidence confirmed what was roughly observed after the unloading of the reactor and deducted from granulometric distributions.

According to the EDS results (not shown here), C was the predominant element in the bed material after the tests, even though appreciably different compositions were detected when comparing the deposited ash particles to the carbonaceous lignite matrix, because the former contained the already recognized elements in the pre-test samples (O, Fe, Na, Mg, Al, Si, S, Cl, K, Ca) .

The average $d_{3,2}$ diameter of char and fly ashes recovered from the filtering candle after test #11 (15.9 μm) was significantly smaller than those of the other materials in Fig. 5. The morphology of char and fly ashes adhering to the surface of the filter candle is shown in Fig. 6 at different magnifications (d: 80×; e: 500×; f: 1000 ×), and the detected chemical composition is visible in the map of Fig. 7, where the main elements are still C, O, and Ca. It is worth noting once again the peculiar affinity between Ca and S to form sulfur compounds [54]. An analogous affinity between Na and Si was also recognizable; this is ascribed to eutectic (low-melting point) mixtures, which are precursors of insidious ash agglomeration phenomena.

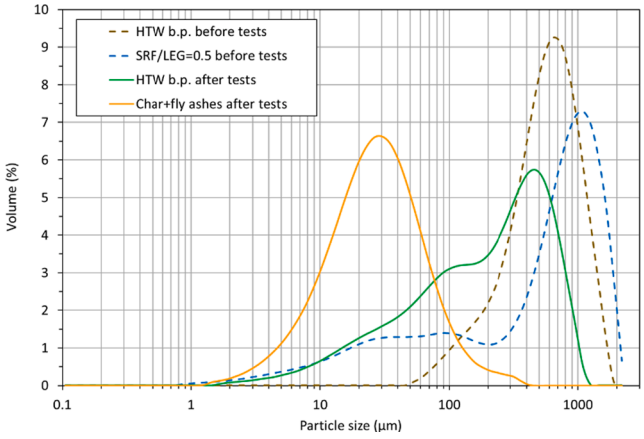

Fig. 5. Particle-size distribution of SRF/LEG = 0.5 before the tests; HTW bottom product (b.p.) before and after tests #10 and #11; char and ashes after tests #10 and #11.

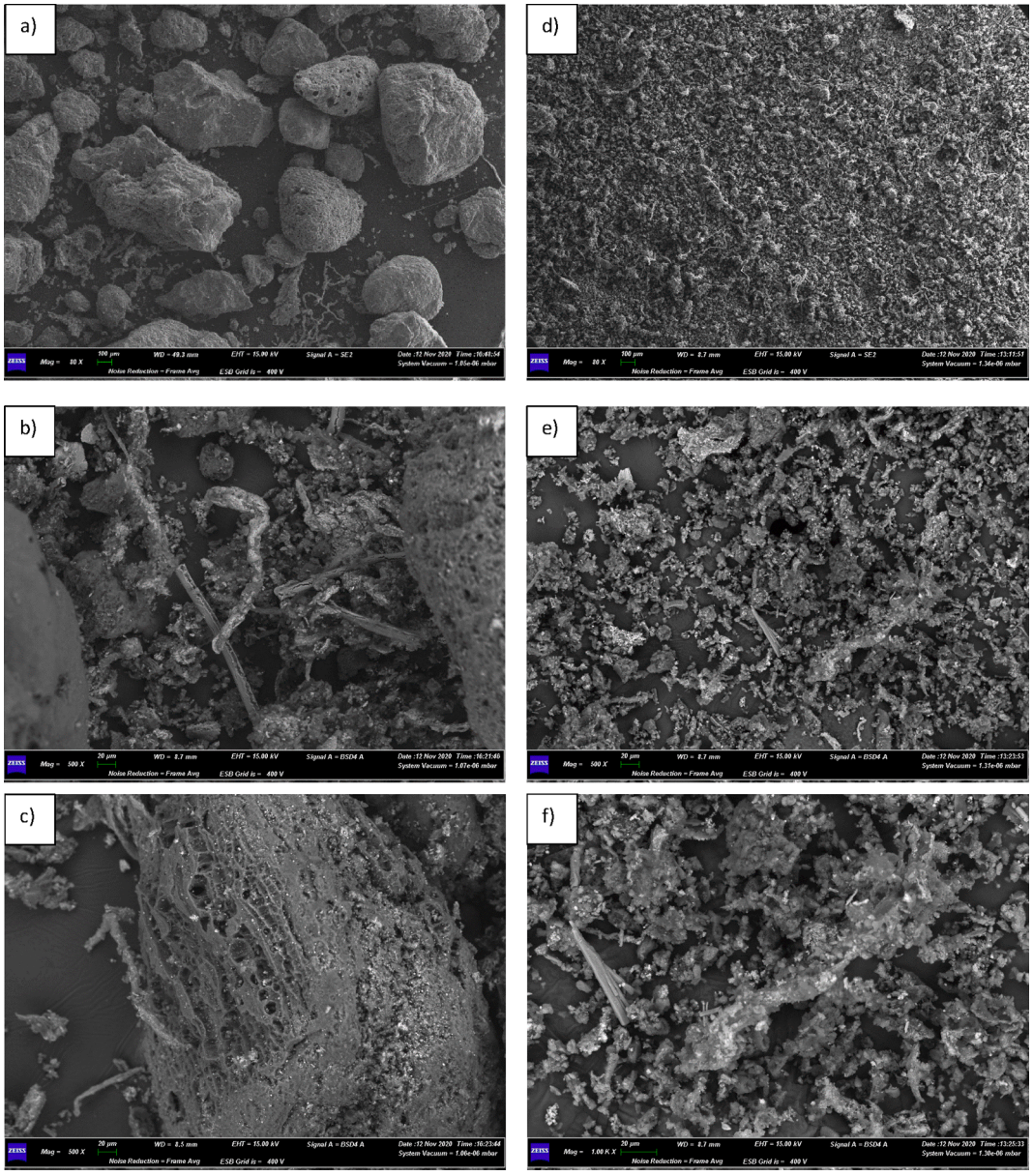

Fig. 6. SEM images of the HTW bottom product after tests #10 and #11, at different magnifications: (a) overview of the sample at 80×, (b) details of residual SRF materials (500 ×), and (c) details of a porous particle (500 ×); SEM images of char and fly ashes adhering to the surface of the filter candle at different magnifications: (d) overview of sample at 80×; details at (e) 500 × and (f) 1000×.

3.4. Pressure-fluctuation analysis

The pressure fluctuations were acquired during the entire experimental campaign to evaluate the bed fluidization quality.

The main evidence regarding the successful tests (Table 3) is summarized in the following discussion. During the heating of the reactor, the PSDF of the fresh bed resulted in two dominant frequencies around 1 and 4 Hz, which were compatible with the desired bubbling fluidization regime. During gasification, the series of low-frequency phenomena (<1 Hz) became more important with a standard deviation of 5.8 mbar; these phenomena were already associated with the peristaltic pump that fed water and (in particular) to the abrupt devolatilization of solid particles, which can occur during the heating step [52,54]. Portions of PSDF from gasification sessions were associated with fluidization phenomena, with locally dominant frequencies between 3 and 4 Hz. Pressure-fluctuation signals acquired after the gasification tests, when water and lignite were no longer fed, indicated that the local dominant frequencies of the bubbling bed returned within the same range, with residual disturbances at frequencies lower than 1 Hz. This implies that the bed particles did not undergo modifications that could alter their fluidization quality, such as sintering or melting with ashes. No de-fluidization phenomena occurred during the successful tests detailed in Table 3. In particular, during tests #10 and #11, the pressure-fluctuation signal was detected and observed online in real time, allowing verification of the continuity of the feeding from the probe and preventing the clogging of the related pipe. Therefore, it was impossible to simultaneously record single files for later analysis.

It is also worth considering the PSDFs and signals acquired during failed tests (tests #2–#5 in Table 2), during which the feeding probe was clogged. During test #2 (Fig. 8a and 8b), the signal indicated good fluidization quality, and in the subsequent acquisitions, changes in the signal became more and more evident, even though the characteristic frequencies were still visible; in test #5 (Fig. 8c and 8d), these frequencies disappeared completely, and the corresponding signals took on

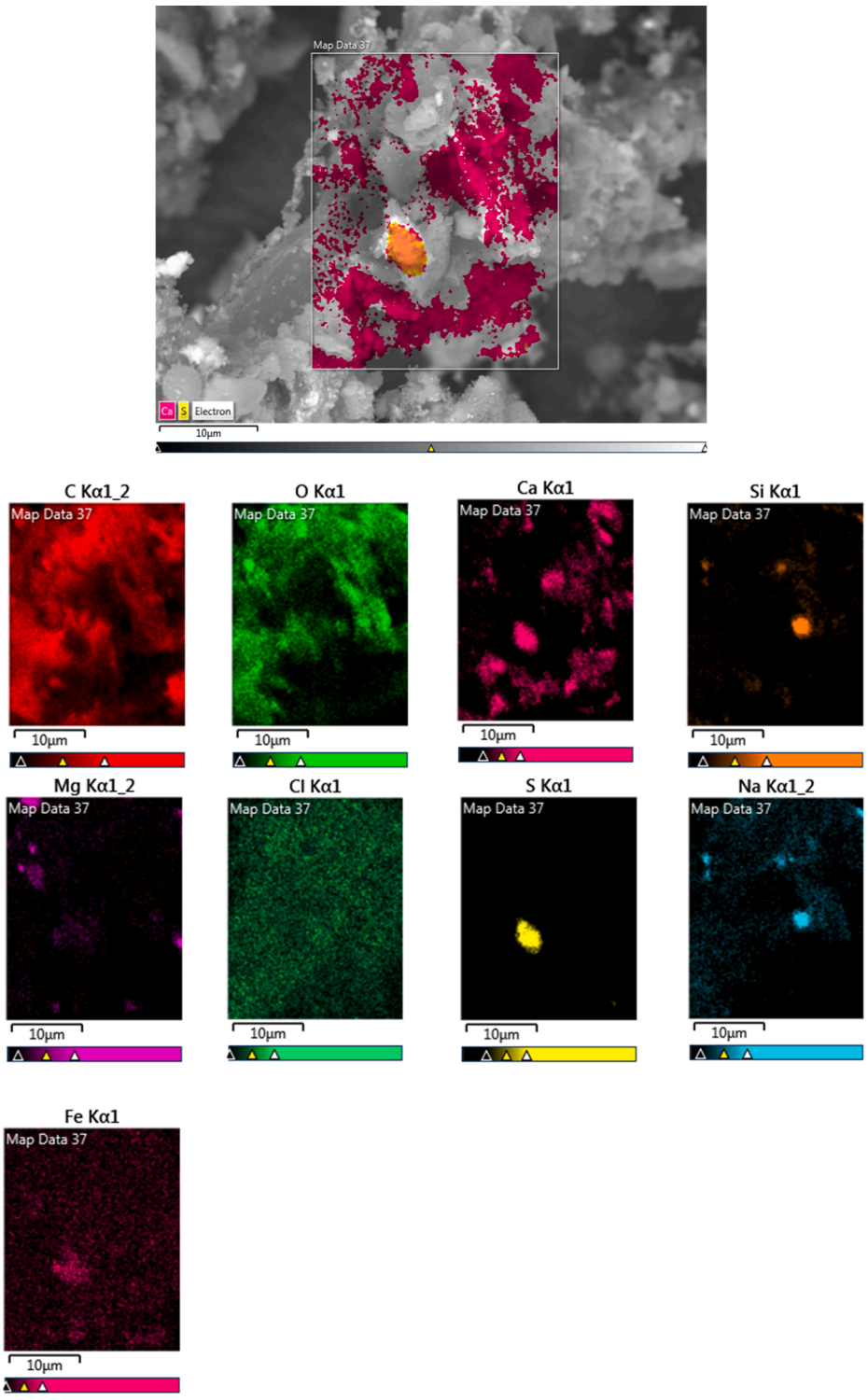

Fig. 7. EDS maps of char and fly ashes recovered on the surface of the filter candle after tests #10 and #11.

a completely different aspect, losing the typical randomization due to the eruption of bubbles on the bed surface. In this example, there was a significant increase in the standard deviation, which was related to sporadic bubbles or puffs of a consumed bed that is starting to sinter; thus, the bed was considered as de-fluidized, in full agreement with experimental observations related to Fig. S1.

These analyses under different fluidization conditions confirmed the potential of the proposed method for prompt diagnosis of the fluid-dynamic bed behavior. It can be implemented as an online control method in gasification plants to detected incipient sintering or de-fluidization phenomena and prevent undesired plant shutdown.

4. Conclusions

Gasification tests were performed in a bench-scale fluidized bed reactor, with the HTW bottom product as the bed material, to mimic the HTW gasification process under realistic operating conditions. The effect of the temperature was examined in tests with three options for solid

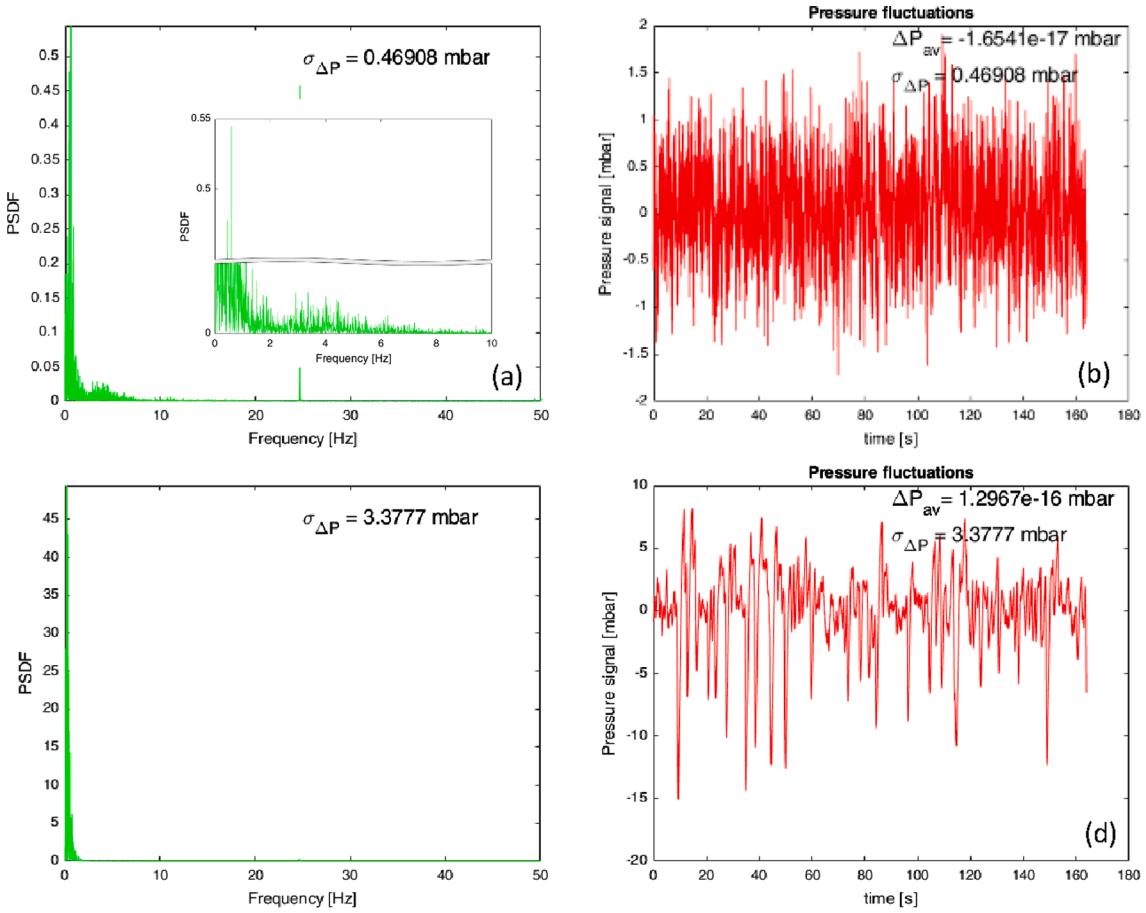

Fig. 8. PSDF and pressure fluctuations signals from the first failed attempts (tests #2 and #5); (a) PSFD of test #2 acquisition with magnification of the 0–10-Hz range and (b) the corresponding pressure-fluctuation signal; (c) PSDF of test #5 acquisition and (d) the corresponding pressure-fluctuation signal.

feed. The product gas quality was improved at higher temperatures, with regard to the water and carbon conversions, cold gas efficiency, and gas yield. Lignite alone or two mixtures of lignite and SRF (SRF/lignite = 0.2 and 0.5 wt/wt) were used to assess the feasibility of co-gasification of waste materials in an HTW fluidized bed reactor. Once the main technical issues related to the feeding of the two fuel mixtures were solved, the obtained results indicated that applying the highest operating temperature (800 °C)—together with proper O_2/fuel and steam/fuel ratios—enhanced the quality of the produced gas, increased the water and carbon conversions and H_2 and CO contents, and reduced the tar content (test #9). In the test with SRF/lignite = 0.2, at 800 °C, despite an uncertainty of 7.7% in the feeding weight, the highest carbon conversion, cold gas efficiency (approximately 93%), gas yield (1.79 Nm^3/kg_{fuel}), and H_2 production (9.07 Nl/min) were achieved.

Gasification of the SRF/lignite = 0.5 wt/wt mixture produced a gas with composition and tar content (8.13 g/Nm^3) close to the results obtained in the gasification tests with lignite alone (6.74 g/Nm^3), although this last value is unexpectedly high.

The pressure-fluctuation analyses did not indicate de-fluidization of the bed when the experimental operations went as planned; thus, it was deduced that no ash melting or agglomeration of the bed material occurred during the regular gasification tests. In contrast, the pressure-fluctuation signals and evidence regarding the bed status for the first failed attempts with SFR/lignite = 0.2 suggested that these phenomena can occur in the case of irregular gasification operations. This highlights the need for an online monitoring system for industrial plants, for which the pressure-fluctuation analysis performed in this study is good candidate.

The particle-size distributions of the fuel and bed materials before and after the tests, together with the related SEM-EDS analyses, highlighted the effectiveness of the proposed SRF grinding procedure, which resulted in complete gasification of the SRF, owing to its higher reactivity and higher content of volatile matter compared with lignite. Under the selected operating conditions, these characterizations also confirmed the absence of sintering and agglomeration of the bed material, in agreement with the pressure-fluctuation diagnoses. In the SEM/EDS analyses, the ashes produced during the gasification tests exhibited an affinity between Ca and S (probably indicating the capacity of Ca to retain S in the ashes), as well as between Na and Si (ascribed to local eutectic mixtures).

The bench-scale gasification tests indicated that the addition of waste material to lignite does not cause significant issues or substantial changes in the gas composition or tar production. These results are promising and can be exploited at the pilot/commercial scale with SRF/lignite = 0.5 in the feedstock and HTW bottom product as the bed material, without issues or significant detriment to the gas quality, if the temperature is strictly controlled and limited to 800 °C.

Declaration of Competing Interest

The authors declare that they have no known competing financial interests or personal relationships that could have appeared to influence the work reported in this paper.

Acknowledgements

The authors gratefully acknowledge the financial support from the European Project LIG2LIQ (RFCS-01-2017 n°796585) co-funded by the

European Commission managed Research Fund for Coal and Steel (RFCS). The authors thank RWE Power AG for supplying lignite, TUDA for supplying the HTW bottom product, and N + P for supplying SRF. ICHPW is also kindly acknowledged for the characterization of lignite and SRF. The authors thank Dr. Alessia Pepe from the University of Teramo for the HPLC analyses, as well as Alessandra Tacconi for her contribution to test #1.

Appendix A. Supplementary data

Supplementary data to this article can be found online at https://doi.org/10.1016/j.fuel.2021.121271.

References

[1] Obama B. The irreversible momentum of clean energy: Private-sector efforts help drive decoupling of emissions and economic growth. Science 2017;355(6321):126–9. https://doi.org/10.1126/science.aam6284.
[2] United Nations. Paris Agreement. 21st Conf Parties 2015:3. https://unfccc.int/process-and-meetings/the-paris-agreement/the-paris-agreement (accessed January 3, 2021).
[3] World Health Organization. COP24 Special report: Health and Climate Change. 2018. https://www.who.int/globalchange/publications/COP24-report-health-climate-change/en/ (accessed January 3, 2021).
[4] A European Green Deal | European Commission. https://ec.europa.eu/info/strategy/priorities-2019-2024/european-green-deal_en (accessed January 3, 2021).
[5] Commission launch the European Just Transition Platform https://ec.europa.eu/commission/presscorner/detail/en/IP_20_1201 (accessed January 15, 2021).
[6] Lig2Liq – Cost Effective Conversion of Lignite and Waste to Liquid Fuels https://www.lig2liq.eu/ (accessed January 3, 2021).
[7] Materazzi M, Foscolo PU. The role of waste and renewable gas to decarbonize the energy sector. Substit Nat Gas from Waste Tech Assess Ind Appl Biochem Thermochem Process 2019. https://doi.org/10.1016/B978-0-12-815554-7.00001-5.
[8] Ferronato N, Torretta V. Waste mismanagement in developing countries: A review of global issues. Int J Environ Res Public Health 2019;16. https://doi.org/10.3390/ijerph16061060.
[9] CLARA – Chemical looping gasification for sustainable production of biofuels https://clara-h2020.eu/ (accessed January 4, 2021).
[10] Lombardi L, Carnevale E, Corti A. A review of technologies and performances of thermal treatment systems for energy recovery from waste. Waste Manag 2015;37:26–44. https://doi.org/10.1016/j.wasman.2014.11.010.
[11] Stiegel GJ, Maxwell RC. Gasification technologies: The path to clean, affordable energy in the 21st century. Fuel Process Technol 2001;71:79–97. https://doi.org/10.1016/S0378-3820(01)00138-2.
[12] Hervy M, Remy D, Dufour A, Mauviel G. Air-blown gasification of Solid Recovered Fuels (SRFs) in lab-scale bubbling fluidized-bed: Influence of the operating conditions and of the SRF composition. Energy Convers Manag 2019;181:584–92. https://doi.org/10.1016/j.enconman.2018.12.052.
[13] Valin S, Ravel S, Pons de Vincent P, Thiery S, Miller H. Fluidized bed air gasification of solid recovered fuel and woody biomass: Influence of experimental conditions on product gas and pollutant release. Fuel 2019;242:664–72. https://doi.org/10.1016/j.fuel.2019.01.094.
[14] Gallucci K, Foscolo PU. Process Intensification for Sustainable Energy Conversion. Chichester, UK: John Wiley & Sons, Ltd; 2015. 10.1002/9781118449394.
[15] Richardson Y, Blin J, Julbe A. A short overview on purification and conditioning of syngas produced by biomass gasification: Catalytic strategies, process intensification and new concepts. Prog Energy Combust Sci 2012;38:765–81. https://doi.org/10.1016/j.pecs.2011.12.001.
[16] Pfeifer C, Koppatz S, Hofbauer H. Steam gasification of various feedstocks at a dual fluidised bed gasifier: Impacts of operation conditions and bed materials. Biomass Convers Biorefinery 2011. https://doi.org/10.1007/s13399-011-0007-1.
[17] Mondol JD, McIlveen-Wright D, Rezvani S, Huang Y, Hewitt N. Techno-economic evaluation of advanced IGCC lignite coal fuelled power plants with CO2 capture. Fuel 2009. https://doi.org/10.1016/j.fuel.2009.04.019.
[18] Wang T, Stiegel G. Integrated gasification combined cycle (IGCC) technologies; 2016. 10.1016/c2014-0-00849-0.
[19] Cormos CC. Integrated assessment of IGCC power generation technology with carbon capture and storage (CCS). Energy 2012. https://doi.org/10.1016/j.energy.2012.03.025.
[20] Kee RJ, Zhu H, Sukeshini AM, Jackson GS. Solid oxide fuel cells: Operating principles, current challenges, and the role of syngas. Combust Sci Technol 2008. https://doi.org/10.1080/00102200801963458.
[21] Wang L, Weller CL, Jones DD, Hanna MA. Contemporary issues in thermal gasification of biomass and its application to electricity and fuel production. Biomass Bioenergy 2008. https://doi.org/10.1016/j.biombioe.2007.12.007.
[22] Venvik HJ, Yang J. Catalysis in microstructured reactors: Short review on small-scale syngas production and further conversion into methanol. DME and Fischer-Tropsch products. Catal Today 2017;285:135–46. https://doi.org/10.1016/j.cattod.2017.02.014.
[23] Wang H, Pei Y, Qiao M, Zong B. Design of Bifunctional Solid Catalysts for Conversion of Biomass-Derived Syngas into Biofuels; 2017, p. 137–58. 10.1007/978-981-10-5137-1_4.
[24] Hofbauer H, Materazzi M. Waste gasification processes for SNG production. Substit Nat Gas from Waste Elsevier 2019:105–60. https://doi.org/10.1016/B978-0-12-815554-7.00007-6.
[25] Weber G, Di Giuliano A, Rauch R, Hofbauer H. Developing a simulation model for a mixed alcohol synthesis reactor and validation of experimental data in IPSEpro. Fuel Process Technol 2016. https://doi.org/10.1016/j.fuproc.2015.05.024.
[26] Yu MM, Masnadi MS, Grace JR, Bi XT, Lim CJ, Li Y. Co-gasification of biosolids with biomass: Thermogravimetric analysis and pilot scale study in a bubbling fluidized bed reactor. Bioresour Technol 2015. https://doi.org/10.1016/j.biortech.2014.10.045.
[27] Masnadi MS, Grace JR, Bi XT, Lim CJ, Ellis N. From fossil fuels towards renewables: Inhibitory and catalytic effects on carbon thermochemical conversion during co-gasification of biomass with fossil fuels. Appl Energy 2015. https://doi.org/10.1016/j.apenergy.2014.12.006.
[28] Habibi R, Kopyscinski J, Masnadi MS, Lam J, Grace JR, Mims CA, et al. Co-gasification of biomass and non-biomass feedstocks: Synergistic and inhibition effects of switchgrass mixed with sub-bituminous coal and fluid coke during CO2 gasification. Energy Fuels 2013. https://doi.org/10.1021/ef301567h.
[29] Masnadi MS, Grace JR, Bi XT, Lim CJ, Ellis N, Li YH, et al. From coal towards renewables: Catalytic/synergistic effects during steam co-gasification of switchgrass and coal in a pilot-scale bubbling fluidized bed. Renew Energy 2015. https://doi.org/10.1016/j.renene.2015.05.044.
[30] Masnadi MS, Grace JR, Bi XT, Lim CJ, Ellis N, Li YH, et al. Single-fuel steam gasification of switchgrass and coal in a bubbling fluidized bed: A comprehensive parametric reference for co-gasification study. Energy 2015. https://doi.org/10.1016/j.energy.2014.11.054.
[31] Masnadi MS, Grace JR, Bi XT, Ellis N, Lim CJ, Butler JW. Biomass/coal steam co-gasification integrated with in-situ CO2 capture. Energy 2015. https://doi.org/10.1016/j.energy.2015.02.028.
[32] Bhoi PR, Huhnke RL, Kumar A, Indrawan N, Thapa S. Co-gasification of municipal solid waste and biomass in a commercial scale downdraft gasifier. Energy 2018. https://doi.org/10.1016/j.energy.2018.08.151.
[33] Mazzoni L, Ahmed R, Janajreh I. Plasma Gasification of Two Waste Streams: Municipal Solid Waste and Hazardous Waste from the Oil and Gas Industry. Energy Procedia 2017. https://doi.org/10.1016/j.egypro.2017.03.882.
[34] Dalai AK, Batta N, Eswaramoorthi I, Schoenau GJ. Gasification of refuse derived fuel in a fixed bed reactor for syngas production. Waste Manag 2009. https://doi.org/10.1016/j.wasman.2008.02.009.
[35] Tanigaki N, Manako K, Osada M. Co-gasification of municipal solid waste and material recovery in a large-scale gasification and melting system. Waste Manag 2012. https://doi.org/10.1016/j.wasman.2011.10.019.
[36] Brems A, Dewil R, Baeyens J, Zhang R. Gasification of plastic waste as waste-to-energy or waste-to-syngas recovery route. Nat Sci 2013. https://doi.org/10.4236/ns.2013.56086.
[37] Recari J, Berrueco C, Abelló S, Montané D, Farriol X. Gasification of two solid recovered fuels (SRFs) in a lab-scale fluidized bed reactor: Influence of experimental conditions on process performance and release of HCl, H2S, HCN and NH3. Fuel Process Technol 2016;142:107–14. https://doi.org/10.1016/j.fuproc.2015.10.006.
[38] Arena U, Di GF. Fluidized bed gasification of industrial solid recovered fuels. Waste Manag 2016;50:86–92. https://doi.org/10.1016/j.wasman.2016.02.011.
[39] Pinto F, André RN, Carolino C, Miranda M, Abelha P, Direito D, et al. Gasification improvement of a poor quality solid recovered fuel (SRF). Effect of using natural minerals and biomass wastes blends. Fuel 2014;117:1034–44. https://doi.org/10.1016/j.fuel.2013.10.015.
[40] Lettieri P, Yassin L, Simons SJR. Advanced thermal treatment of composite wastes for energy recovery. Manag Recycl Reuse Waste Compos 2009. https://doi.org/10.1533/9781845697662.2.152.
[41] Patel C, Lettieri P, Germanà A. Techno-economic performance analysis and environmental impact assessment of small to medium scale SRF combustion plants for energy production in the UK. Process Saf Environ Prot 2012;90:255–62. https://doi.org/10.1016/j.psep.2011.06.015.
[42] Courson C, Gallucci K. Gas cleaning for waste applications (syngas cleaning for catalytic synthetic natural gas synthesis). Substit Nat Gas from Waste, Elsevier 2019:161–220. https://doi.org/10.1016/B978-0-12-815554-7.00008-8.
[43] Belgiorno V, Feo G De, Rocca C Della, Napoli RMA. Energy from gasification of solid wastes 2003;23:1–15.
[44] Arena U. Process and technological aspects of municipal solid waste gasification. A review. Waste Manag 2012;32:625–39. https://doi.org/10.1016/j.wasman.2011.09.025.
[45] Arena U, Di Gregorio F. Gasification of a solid recovered fuel in a pilot scale fluidized bed reactor. Fuel 2014;117:528–36. https://doi.org/10.1016/j.fuel.2013.09.044.
[46] Arena U, Di Gregorio F. Fluidized bed gasification of industrial solid recovered fuels. Waste Manag 2016;50:86–92. https://doi.org/10.1016/j.wasman.2016.02.011.
[47] Bridgwater AV. The technical and economic feasibility of biomass gasification for power generation. Fuel 1995. https://doi.org/10.1016/0016-2361(95)00001-L.
[48] Corella J, Herguido J, Gonzalez-Saiz J, Alday FJ, Rodriguez-Trujillo JL. Fluidized Bed Steam Gasification of Biomass with Dolomite and with a Commercial FCC Catalyst. Res Thermochem Biomass Convers 1988. https://doi.org/10.1007/978-94-009-2737-7_57.

[49] Motta IL, Miranda NT, Maciel Filho R, Wolf Maciel MR. Biomass gasification in fluidized beds: A review of biomass moisture content and operating pressure effects. Renew Sustain Energy Rev 2018. https://doi.org/10.1016/j.rser.2018.06.042.
[50] Heidenreich S, Müller M, Foscolo PU. Advanced Biomass Gasification: New Concepts for Efficiency Increase and Product Flexibility. Elsevier Inc.; 2016. 10.1016/C2015-0-01777-4.
[51] Knoef HAM. Handbook on Biomass Gasification. BTG Biomass Technology Group BV; 2nd edition (January 1, 2012) ISBN-10 : 9081938509; ISBN-13 : 978-9081938501.
[52] Savuto E, Di Carlo A, Gallucci K, Di Giuliano A, Rapagnà S. Steam gasification of lignite and solid recovered fuel (SRF) in a bench scale fluidized bed gasifier. Waste Manag 2020;114:341–50. https://doi.org/10.1016/j.wasman.2020.07.016.
[53] Krause D, Herdel P, Ströhle J, Epple B. HTWTM-gasification of high volatile bituminous coal in a 500 kWth pilot plant. Fuel 2019;250:306–14. https://doi.org/10.1016/j.fuel.2019.04.014.
[54] Savuto E, May J, Di Carlo A, Gallucci K, Di Giuliano A, Rapagnà S. Steam gasification of lignite in a bench-scale fluidized-bed gasifier using olivine as bed material. Appl Sci 2020;10:2931. https://doi.org/10.3390/APP10082931.
[55] Di Giuliano A, Foscolo PU, Di Carlo A, Steele A, Gallucci K. Kinetic Characterization of Tar Reforming on Commercial Ni-Catalyst Pellets Used for In Situ Syngas Cleaning in Biomass Gasification: Experiments and Simulations under Process Conditions. Ind Eng Chem Res 2020. https://doi.org/10.1021/acs.iecr.0c05131.
[56] CEN/TS 15439:2006 Biomass Gasification - Tar and Particles in Product Gases. Sampling and Analysis.
[57] Di Marcello M, Gallucci K, Rapagnà S, Gruber R, Matt M. HPTLC and UV spectroscopy as innovative methods for biomass gasification tars analysis. Fuel 2014;116:94–102. https://doi.org/10.1016/j.fuel.2013.07.117.
[58] Gallucci K, Gibilaro LG. Dimensional Cold-Modeling Criteria for Fluidization Quality. Ind Eng Chem Res 2005;44:5152–8. https://doi.org/10.1021/ie049407t.
[59] Di Giuliano A, Funcia I, Pérez-Vega R, Gil J, Gallucci K. Novel application of pretreatment and diagnostic method using dynamic pressure fluctuations to resolve and detect issues related to biogenic residue ash in chemical looping gasification. Processes 2020. https://doi.org/10.3390/PR8091137.
[60] Bartels M, Lin W, Nijenhuis J, Kapteijn F, van Ommen JR. Agglomeration in fluidized beds at high temperatures: Mechanisms, detection and prevention. Prog Energy Combust Sci 2008;34:633–66. https://doi.org/10.1016/j.pecs.2008.04.002.
[61] Korbee R, Van Ommen JR, Lensselink J, Nijenhuis J, Kiel JHA, Van Den Bleek CM. Early Agglomeration Recognition System (EARS). J Energy Resour Technol Trans ASME 2006;128:143–8. https://doi.org/10.1115/1.2191505.
[62] van Ommen JR, Coppens M-O, van den Bleek CM, Schouten JC. Early warning of agglomeration in fluidized beds by attractor comparison. AIChE J 2000;46:2183–97. https://doi.org/10.1002/aic.690461111.
[63] Herdel P, Krause D, Peters J, Kolmorgen B, Ströhle J, Epple B. Experimental investigations in a demonstration plant for fluidized bed gasification of multiple feedstock's in 0.5 MW th scale. Fuel 2017;205:286–96. https://doi.org/10.1016/j.fuel.2017.05.058.
[64] Scala F, Chirone R. An SEM/EDX study of bed agglomerates formed during fluidized bed combustion of three biomass fuels. Biomass Bioenergy 2008. https://doi.org/10.1016/j.biombioe.2007.09.009.
[65] Savuto E, Di Carlo A, Steele A, Heidenreich S, Gallucci K, Rapagnà S. Syngas conditioning by ceramic filter candles filled with catalyst pellets and placed inside the freeboard of a fluidized bed steam gasifier. Fuel Process Technol 2019;191:44–53. https://doi.org/10.1016/j.fuproc.2019.03.018.
[66] Basu P. Combustion and gasification in fluidized beds. CRC/Taylor & Francis; 2006.
[67] Weiland F, Lundin L, Celebi M, van der Vlist K, Moradian F. Aspects of chemical recycling of complex plastic waste via the gasification route. Waste Manag 2021;126:65–77. https://doi.org/10.1016/j.wasman.2021.02.054.
[68] Zaccariello L, Mastellone M. Fluidized-Bed Gasification of Plastic Waste, Wood, and Their Blends with Coal. Energies 2015;8:8052–68. https://doi.org/10.3390/en8088052.
[69] Liakakou ET, Vreugdenhil BJ, Cerone N, Zimbardi F, Pinto F, André R, et al. Gasification of lignin-rich residues for the production of biofuels via syngas fermentation: Comparison of gasification technologies. Fuel 2019;251:580–92. https://doi.org/10.1016/j.fuel.2019.04.081.
[70] Rapagnà S, Virginie M, Gallucci K, Courson C, Di Marcello M, Kiennemann A, et al. Fe/olivine catalyst for biomass steam gasification: Preparation, characterization and testing at real process conditions. Catal Today 2011. https://doi.org/10.1016/j.cattod.2010.11.098.